Optical vibrations in the Zn_3P_2 lattice

1989 J. Phys.: Condens. Matter 1 9283

(http://iopscience.iop.org/0953-8984/1/47/002)

J. Phys.: Condens. Matter 1 (1989) 9283–9299. Printed in the UK

Optical vibrations in the Zn_3P_2 lattice

Jan Misiewicz
Institute of Physics, Technical University of Wrocław, Wybrzeże Wyspiańskiego 27, 50-370 Wrocław, Poland

Received 22 June 1988, in final form 28 April 1989

Abstract. Optical vibrations in Zn_3P_2 crystals were investigated using reflectivity spectra in the 40–400 cm^{-1} wavenumber range, absorption spectra in the 380–1200 cm^{-1} range and Raman scattering spectra in the 25–500 cm^{-1} range. From these the energies of the one-phonon and multi-phonon transitions were determined. The symmetry of phonon branches through the symmetry lines and points in the Zn_3P_2 Brillouin zone were determined using group theory analysis. The selection rules of the overtones and combinations permitted in infrared and/or Raman spectra were derived and used to interpret the observed multi-phonon transitions.

1. Introduction

Among relatively new semiconducting materials, Zn_3P_2 has recently become one of the most promising. The growing interest in this compound is due to its possible application as a solar energy converter. For Zn_3P_2 the conditions necessary for solar energy converters are fulfilled; the location of the optical absorption edge at 1.5–1.6 eV (Pawlikowski *et al* 1979, Fagen 1979, Misiewicz and Gaj 1981, Pawlikowski 1982) is close to the optimum value determined by theoretical analysis (Loferski 1956), the minority-carrier diffusion length is approximately 10 μm (Nauka and Misiewicz 1981) and finally the elements constituting the compound are abundant and cheap. The results of Zn_3P_2 applications as photovoltaic photoconverters have been summarised by Pawlikowski (1988a, b).

Ultraviolet detectors were made using thin Zn_3P_2 films by Bendett and Hunspreger (1981).

Distinct photodichroism was observed for metal–Zn_3P_2 (oriented single-crystal) junctions that were applied in a light polarisation step indicator (Misiewicz *et al* 1984).

Zn_3P_2 is a very interesting compound both because of its application and because its basic properties are relatively little known. The present paper is devoted to Zn_3P_2 lattice vibrations. Until now, there have been only a few papers in which results on this problem have been presented. Chronologically, the first infrared transmission measurement in the 400–750 cm^{-1} wavenumber range was made by Radautsan *et al* (1977) at room temperature. A few lattice bands were found in this region, with very small resolution. The absorption spectra in the 500–1000 cm^{-1} range were measured by Misiewicz *et al* (1986a) at 295 and 80 K; 12 absorption bands were observed. Restrahlen spectrum of Zn_3P_2 at room temperature and multiphonon absorption measurements in the 40–700 cm^{-1} range were presented by Misiewicz *et al* (1988).

0953-8984/89/479283 + 17 $02.50

The aim of this paper is to present an analysis of electromagnetic wave interaction with the lattice of Zn_3P_2. Group theory methods are used in these considerations. Critical point analysis and compatibility relations allow us to determine the symmetry of phonon dispersion curves. Two-phonon selection rules for infrared- and Raman-active modes are determined on the basis of Kronecker symmetrised square and Kronecker product reductions. Theoretical predictions are used in the analysis of experimental results. Fundamental reflectivity spectra are presented at room temperature and liquid-helium temperature in the 40–450 cm^{-1} range. Absorption spectra in the multi-phonon transition region (380–1200 cm^{-1}) are presented at room temperature and a low temperature. The Raman scattering is measured in the range 25–500 cm^{-1}.

2. Crystal structure

Zn_3P_2 is one of four crystallographically similar semiconductors of the type $A_3^{II}B_2^{V}$, the others, being Cd_3P_2, Zn_3As_2 and Cd_3As_2 (Żdanowicz and Żdanowicz 1975). Both Zn_3P_2 and Cd_3P_2 as well as Zn_3As_2 and Cd_3As_2 are strictly isostructural (Pistorius *et al* 1977). According to the papers by Stackelberg and Paulus (1935) and Pistorius *et al* (1977) the Zn_3P_2 lattice possesses tetragonal symmetry, belonging to space group D_{4h}^{15} ($P4_2nmc$). The unit-cell dimensions are $a = b = 8.0889$ Å and $c = 11.4069$ Å (Pistorius *et al* 1977) it contains eight formula units and 40 atoms. The crystal structure of Zn_3P_2 in the first approximation may be regarded as a Na_2O lattice (or anti-fluoride lattice) in which one quarter of the metal sites are vacant. As in the prototypical anti-fluoride structure, cations and anions occupy alternate planes normal to the c axis, and the anion sublattice is nearly close packed (FCC), which is a condition for semiconducting properties (Mooser and Pearson 1961). In this case, however, cation vacancies occur in pairs along all four body diagonals of the anti-fluoride subcell. The ordering of cation vacancies makes the

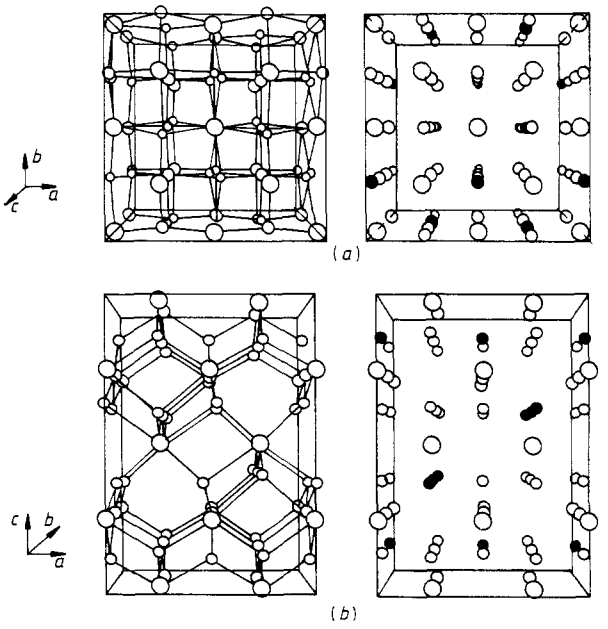

Figure 1. Perspective view of the unit cell and contents for Zn_3P_2 in an ideal anti-fluoride structure in the two main directions (*a*) perpendicular and (*b*) parallel to the c axis, respectively. Zn atoms are indicated by the smaller circles and P atoms by the larger circles. Vacancy sites are indicated by full circles (Pistorius *et al* 1977).

volume of the Zn_3P_2 unit cell four times the volume of the anti-fluoride subcell and gives the lowered symmetry. Because of the vacancies in the crystal structure, there occur certain distortions. The Zn atoms are tetrahedrally coordinated with phosphorus atoms; their nearest neighbours are at the corners of a distorted tetrahedron. Every phosphorus atom is surrounded by zinc atoms located on six corners of a slightly distorted cube. Figure 1 shows a comparison of an ideal arrangement of anti-fluoride structure with the real crystal structure of Zn_3P_2 (Pistorius *et al* 1977). According to the same paper the ideal interatomic distances are equal to 2.48 Å for Zn–P and 4.05 Å for P–P. The displacements between the ideal and real positions are smaller than 0.3 Å for the Zn–P distances and 0.1 Å for the P–P distances. The angular deviations are smaller than 7.5° from the ideal value.

3. Theoretical analysis of lattice modes

3.1. Symmetry of one-phonon branches

A Zn_3P_2 crystal composed of 40 atoms possesses 120 phonon branches, 117 of them being optical (oscillation) and three acoustic modes, i.e. pure translations.

The phonons from the regions of the Brillouin zone where the density of phonon states per unit wavevector is high are the only ones in each branch to participate in optical processes. These regions, or points, are known as critical points in the phonon dispersion. At the branch critical point the phonon frequency as a function of wavevector has a vanishing slope or changes sign discontinuously in one or more directions. The number of phonons in the crystal which can participate in optical processes is the sum of products of the numbers of critical points for that space group multiplied by the numbers of distinct branches at each critical point. Each of these phonons must be assigned to one of the irreducible representations of the crystal space group, i.e. it must belong to the so-called crystal species. Using the space group theory it is then possible to determine the optical activity of the phonons.

The first Brillouin zone of the Zn_3P_2 crystal due to its symmetry D_{4h}^{15} is formed as a parallelepiped as presented in figure 2. The high-symmetry points and lines in the irreducible part of the Brillouin zone are marked in this figure. According to general rules (Birman 1984), most of the critical points are those at the centre and the boundaries of the Brillouin zone, and they are placed at the high-symmetry points. The Γ point, as

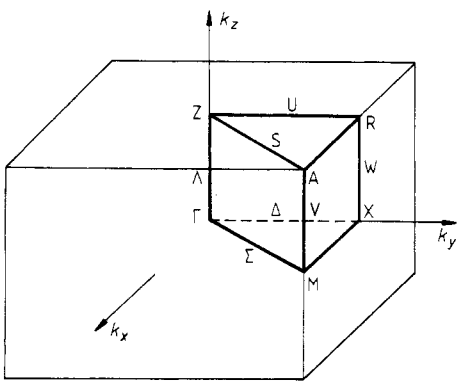

Figure 2. The first Brillouin zone of Zn_3P_2 with the representation domain, and the high-symmetry point and lines indicated.

well as the Z, A and M points, possess the highest symmetries; the X and R points and the Σ, Λ and Δ lines possess lower symmetries.

Let us start with the Γ point. At this point there exist only infinite-wavelength phonons. The distribution of the total number of 120 phonon branches between irreducible representations of the D_{4h}^{15} space group can be determined on the basis of the factor group analysis proposed by Fateley *et al* (1971). The total irrreducible representation of the crystal is the combined irreducible representation of each equivalent set of atoms. Starting from the site symmetry groups of the constituent elements, one correlates the irreducible representations of the site symmetry groups with those of the crystal factor group. For Zn_3P_2, the D_{4h} point group is a factor group. According to Stackelberg and Paulus (1935) and Pistorius *et al* (1977), the phosphorus atoms occupy two sets of the equivalent positions of C_{2v} symmetry, each of multiplicity 4, and one set of the C_2 position with multiplicity 8. Zinc atoms occupy three sets of C_s (C_{1h}) symmetry positions with multiplicity 8. Performing the correlation procedure, we obtain the total distribution of the Zn_3P_2 lattice modes among the irreducible representations of the factor group as follows in the notation of Bouckaert *et al* (1936):

$$\Gamma = 9\Gamma_1^+ + 4\Gamma_1^- + 5\Gamma_2^+ + 10\Gamma_2^- + 10\Gamma_3^+ + 5\Gamma_3^- + 4\Gamma_4^+ + 9\Gamma_4^- + 16\Gamma_5^+ + 16\Gamma_5^- \tag{1}$$

and, in the Mulliken (1933) notation,

$$\Gamma = 9A_{1g} + 4A_{1u} + 5A_{2g} + 10A_{2u} + 10B_{1g} + 5B_{1u} + 4B_{2g} + 9B_{2u} + 16E_g + 16E_u .$$

The notation of Bouckaert *et al* will be used here. For infrared dipole interaction the ∇ operator of the transition matrix element

$$\Gamma_2^- + \Gamma_5^- . \tag{2}$$

So the representation of infrared-active one-phonon modes is found to be

$$\Gamma^{IR} = 9\Gamma_2^- + 15\Gamma_5^- . \tag{3}$$

The pure translations, i.e. acoustic modes, also possess $\Gamma_2^- + \Gamma_5^-$ symmetry but they vanish at the Γ point. The polarisability tensor, which is responsible for the Raman scattering process, in the D_{4h}^{15} structure possesses components as follows (Loudon 1964):

$$\underset{\Gamma_1^+}{\begin{pmatrix} a & . & . \\ . & a & . \\ . & . & b \end{pmatrix}} \underset{\Gamma_3^+}{\begin{pmatrix} a & . & . \\ . & -c & . \\ . & . & . \end{pmatrix}} \underset{\Gamma_4^+}{\begin{pmatrix} . & d & . \\ d & . & . \\ . & . & . \end{pmatrix}} \underbrace{\begin{pmatrix} . & . & e \\ . & . & . \\ e & . & . \end{pmatrix} \begin{pmatrix} . & . & . \\ . & . & e \\ . & e & . \end{pmatrix}}_{\Gamma_5^+} \tag{4}$$

and so we obtain the Raman-active one-phonon modes

$$\Gamma^R = 9\Gamma_1^+ + 10\Gamma_3^+ + 4\Gamma_4^+ + 16\Gamma_5^+ . \tag{5}$$

Group theory analysis allows us to evaluate the phonon branches throughout the Brillouin zone. We can distribute the 120 one-phonon modes between irreducible representations of the symmetry points and lines. For the high-symmetry points we obtain

$$\begin{aligned} Z &= 16Z_1 + 16Z_2 + 9Z_3 + 19Z_4 \\ A &= 14A_1 + 14A_2 + 16A_3 + 16A_4 \\ M &= 16M_1 + 16M_2 + 14M_3 + 14M_4 \\ R &= 25R_1 + 35R_2 \\ X &= 25X_1 + 35X_2 . \end{aligned} \tag{6}$$

All these irreducible representations are double degenerate. By means of the compatibility relations, determined according to the standard procedure of representation decomposition (see, e.g., Streitwolf 1967, Birman 1984), a schematic model of the phonon branch symmetry evaluated through the Brillouin zone is proposed in figure 3. The Kovalev (1965) tables of irreducible representations are used. In this figure, only infrared- or Raman-active modes are included. The branches are developed from Γ to Γ through X, R and Z points (ΓΔXWRUZΛΓ) and from Γ to Z (ΓΣMVASZ) (see also figure 2). It should be mentioned that group theory does not make it possible to choose between representations A_i and A_j at the A point and between Z_i and Z_j representations at the Z point (going from M to Z). The same ambiguity takes place at the W line (see figure 3).

3.2. Two-phonon transitions

The general wavevector conservation rule requires that in both the sum and the difference of phonons their wavevectors must be equal to zero. This condition is fulfilled at the Γ point and, owing to symmetry properties, at the above-listed critical points. If in a two-phonon process the two modes belong to different irreducible representations, one has a combination state. If they are partners of the same space group of irreducible representations, one has an overtone state. For combination states the transition is allowed if the Kronecker product of the irreducible representations is common with the ∇ vector representation (for the infrared dipole allowed transitions) or with the polarisability tensor representation (for the Raman allowed transitions). For overtone states the symmetrised Kronecker square of the phonon irreducible representations must be used to determine the selection rules (Birman 1984, Streitwolf 1965).

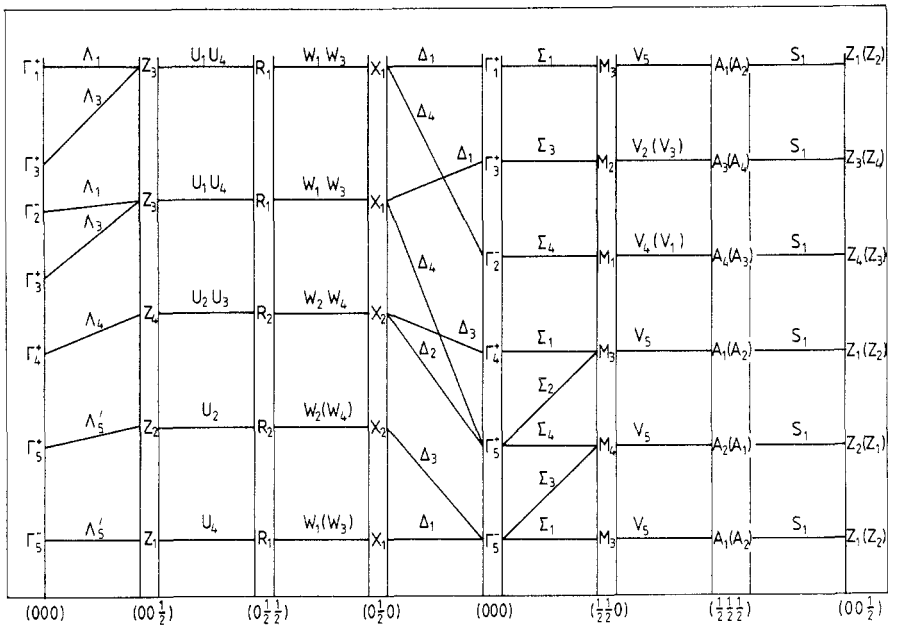

Figure 3. Schematic model of the phonon branches symmetry through the symmetry points and lines of the Brillouin zone. Coordinates of the symmetry point in $2\pi(1/a, 1/a, 1/c)$.

Table 1. Two-phonon processes in Zn_3P_2 at the Γ point.

IR allowed					
			Combinations		
Species	$\Gamma_2^- \otimes \Gamma_1^+$	$\Gamma_2^- \otimes \Gamma_5^+$	$\Gamma_5^- \otimes \Gamma_5^+$	$\Gamma_5^- \otimes \Gamma_i^+$	$i = 1, 3, 4$
Polarisation	Γ_2^-	Γ_5^-	Γ_2^-	Γ_5^-	

Raman allowed					
		Overtones		Combinations	
Species	$[\Gamma_2^-]_{(2)}$	$[\Gamma_5^-]_{(2)}$	$[\Gamma_i^+]_{(2)}$ $i = 1, 3, 4, 5$	$\Gamma_1^+ \otimes \Gamma_i^+$ $i = 3, 4, 5$	$\Gamma_5^+ \otimes \Gamma_i^+$ $i = 3, 4$
Polarisation	Γ_1^+	$\Gamma_1^+, \Gamma_3^+, \Gamma_4^+$	Γ_1^+	Γ_i^+	Γ_5^+

As the first result we obtain that all two-phonon overtones are infrared dipole forbidden and Raman allowed. Such a situation is typical in crystals possessing inversion symmetry (Birman 1984, Streitwolf 1967). Infrared dipole permitted combinations as well as overtones and combinations allowed in Raman scattering processes are presented in table 1. By means of the same method the selection rules for two-phonon processes at the Z, A, M, R and X critical points are determined. The results are collected in table 2.

At the Γ point, from the 60 possible transitions, only six of them are infrared and 13 are Raman permitted by the group theory selection rules. At the high-symmetry points we obtain the numbers of two-phonon optical active modes as 16 infrared and 29 Raman allowed. Other combinations expected between the branches from the different critical points are not considered in this paper.

Table 2. Two-phonon processes in Zn_3P_2 at high symmetry points

IR allowed						
			Overtones			
Species	$[Z_i]_{(2)}$	$i = 3, 4$	$[M_i]_{(2)}$ $i = 1, 2$	$[Q_i]_{(2)}$ $Q = R, X$	$i = 1, 2$	
Polarisation	Γ_2^-		Γ_2^-	Γ_2^-, Γ_5^-		
			Combinations			
Species	$Q_1 \otimes Q_2$	$P_3 \otimes P_4$	$K_1 \otimes K_2$, $K = R, X$	$Q_i \otimes Q_j$	$Q = Z, A, M$; $P = A, M$	
Polarisation	Γ_2^-	Γ_2^-	Γ_5^-	Γ_5^-	$i = 1, 2$; $j = 3, 4$	

Raman allowed						
			Overtones			
Species	$[Z_i]_{(2)}$	$[A_i]_{(2)}$	$[A_j]_{(2)}$	$[M_i]_{(2)}$	$[Q_i]_{(2)}$	$Q = R, X$
Polarisation	Γ_1^+, Γ_3^+ $i = 1, 2, 3, 4$	Γ_1^+ $i = 1, 2$	Γ_3^+, Γ_4^+ $j = 3, 4$	Γ_1^+, Γ_4^+ $i = 1, 2, 3, 4$	$\Gamma_1^-, \Gamma_3^+, \Gamma_5^+$ $i = 1, 2$	
			Combinations			
Species	$Z_3 \otimes Z_4$	$A_3 \otimes A_4$	$M_3 \otimes M_4$	$K_1 \otimes K_2$	$P_1 \otimes P_2$	$Q_1 \otimes Q_2$ $Q_i \otimes Q_j$
Polarisation	Γ_4^+	Γ_1^+	Γ_3^+	Γ_4^+ $K = Z, A$	Γ_3^+ $P = A, M$	Γ_4^+, Γ_5^+ Γ_5^+ $Q = R, X$ $Q = Z, A, M$ $i = 1, 2$ $j = 3, 4$

4. Experimental results

Single Zn_3P_2 crystals were grown by the directed physical transport method described in detail by Misiewicz and Królicki (1985) and Misiewicz *et al* (1986b). The sample oriented by means of X-rays were cut from an ingot, mechanically polished and finally etched in bromine solution in methanol. High-resistivity crystals with a hole concentration p in the range of 10^{13} cm^{-3} at room temperature were used.

4.1. Reflectivity and absorption spectra

Reflectivity spectra were measured at room temperature and 10 K in the 40–450 cm^{-1} wavenumber range (Misiewicz *et al* 1988, Wrobel and Misiewicz 1989). Absorption spectra in the 380–1200 cm^{-1} range at the same temperature were determined using transmission and reflectivity values. Measurements were done using a Bruker model Fourier interferometer and Beckman spectrophotometer. Unpolarised light was applied in these measurements.

Figure 4 presents reflectivity spectra in the reststrahlen region at 295 and 10 K. As is expected, a complex reflectivity structure is observed. In the whole wavenumber range, three regions can be found in the reflectivity spectra. The first (40–115 cm^{-1}) consists of six peaks visible at room temperature. At low temperatures the structure becomes clearer. The relatively broad peak at around 100 cm^{-1} splits into two independent peaks. The second set of very prominent features is located at 240–360 cm^{-1}. We observed five relatively broad maxima at room temperature and seven sharper peaks at 10 K. In between these ranges a relatively flat reflectivity plot is seen. At room temperature, only a few weak transitions in the range 150–185 cm^{-1} can be found (see also the previous paper by Misiewicz *et al* (1988)). A decrease in the temperature causes the two maxima in this region to increase. A more detailed analysis of the temperature dependence of reststrahlen spectra will be published by Wrobel and Misiewicz (1989).

An analysis of the measured reflectivity spectra was performed by means of the Kramers–Kronig method and the spectral dependences of the dielectric constants were determined. According to Barker (1970), the energies of the transverse optical (TO) and longitudinal optical (LO) modes are determined from the maxima positions in the imaginary parts of the dielectric constant and the energy loss function. Table 3 collects the TO and LO phonon energies appropriate to Brillouin zone centre. Thirteen pairs of

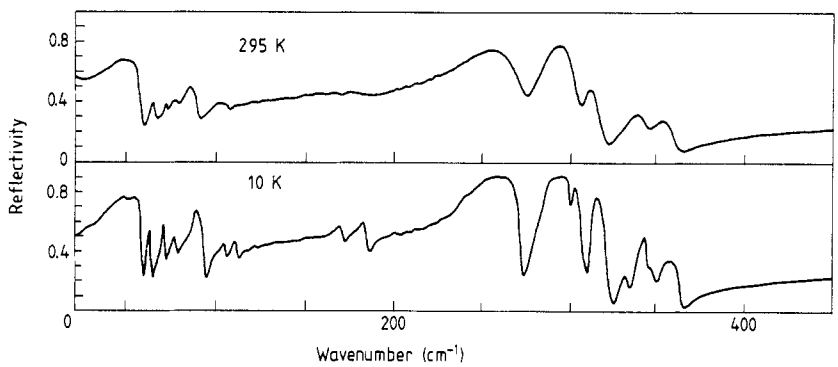

Figure 4. Reflectivity spectra of Zn_3P_2 in the reststrahlen region.

Table 3. Zone-centre infrared-active phonons in Zn_3P_2 (in cm^{-1}).

	Temperature 295 K												
No.	1	2	3	4	5	6	7	8	9	10	11	12	13
TO	44	64	70.5	78	86	103	168.5	182.5	246	285	309.5	338	351
LO	57	66	71	78.5	89	104.5	169	184	276	307	320	345	360

	Temperature 10 K															
No.	1	2	3	4	5	6	7	8	9	10	11	12	13	14	15	16
TO	46.5	62	71	77	87.5	104	110.5	170.5	184	243	285	301.5	312.5	331.5	340	354
LO	58.5	63.7	71.5	78	94	105.5	112.5	172	186	274	309.5	301.5	323	333	348.5	363

Table 4. Energies of zone-centre one-phonon transitions in Zn_3P_2 Raman spectra (in cm^{-1})

No.	1	2	3	4	5	6	7	8	9	10	11	12	13	14	15	16	17	18	19	20
VH	26	34.5	39	45	51	61.5	70	79	84		92	109	120	132	141		151.5		168.5	
VV	27.5		37	45	50	61.5	70			86.5	93					144		159		171

No.	21	22	23	24	25	26	27	28	29	30	31	32	33	34	35	36	37	38	39
VH	188		205		222		231.5	241.5		263	290	306.5		328.5		336		352	363
VV		190.5		212		224.5			258		292		310.5		331		345		363

phonons at 295 K and 16 pairs at 10 K were found: this remains in accordance with the numbers of reflectivity peaks.

The absorption coefficient was determined for wavenumbers higher than 385 cm^{-1} at 295 K and 450 cm^{-1} at 10 K. At room temperature a row of steps is visible in the range 385–550 cm^{-1} (figure 5(*a*)). The local absorption maxima are located in the ranges close to 580 and 680 cm^{-1}. This structure, in general, is reproduced at low temperatures but the absorption background is much smaller than at 295 K (figure 5(*b*)). There are 14 transitions visible at 295 K and at least 25 of them at 10 K in the 454–720 cm^{-1} range. The main maxima close to 580 and 680 cm^{-1} are, at low temperatures, shifted towards higher energies in comparison with room-temperature spectra. Figure 6 presents the higher-energy part of the multi-phonon transition region. The fine structure in the absorption plot in this region is visible only for high-quality and low-concentration samples. The spectra at room temperature and 10 K are similar. A lower absorption background and more visible absorption features are noticed at 10 K. On decrease in temperature a high-energy shift of the prominent structures also exists. For wavenumbers higher than 1250 cm^{-1} there is the beginning of an acceptor photoionisation process (Misiewicz *et al* 1986a).

4.2. Raman scattering spectra

The Raman scattering spectra of Zn_3P_2 were measured in back-scattering geometry at room temperature using polarised light. A krypton ion laser beam with a power of 0.5 W at 676 nm wavelength was employed. A 3–4 m double-grating Spex spectrometer, a cooled GaAs photomultiplier and a photon-counting system were used for collecting the spectra. The scattered light was detected in the 25–500 cm^{-1} range. Measurements were performed under the following conditions: $\boldsymbol{e} \perp \boldsymbol{c} \perp \boldsymbol{e}$ and $\boldsymbol{e} \perp \boldsymbol{c} \parallel \boldsymbol{e}$, where $\boldsymbol{e}$ is the electric vector of the incident and scattered light and $\boldsymbol{c}$ the tetragonal axis of the crystal.

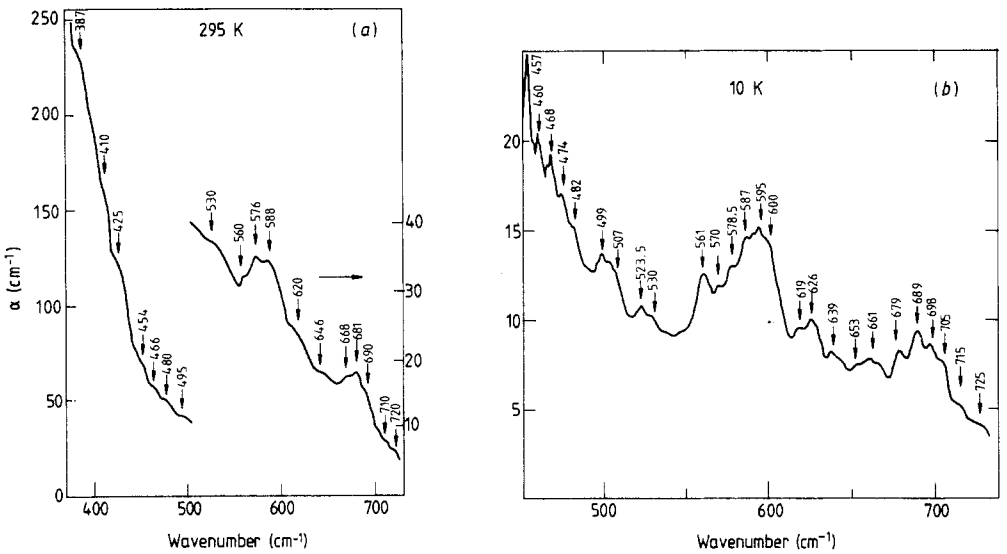

Figure 5. Absorption coefficient spectra of Zn_3P_2 in the two-phonon range at (*a*) room temperature and (*b*) 10 K.

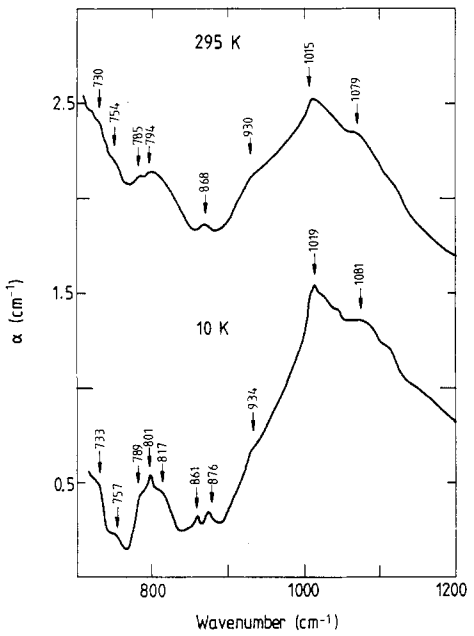

Figure 6. Absorption coefficient spectra of Zn_3P_2 in the three-phonon range at room temperature and 10 K.

These notations are equivalent to the following: $y(xx)\bar{y}$ or $x(yy)\bar{x}$ (VV) and $y(xz)\bar{y}$ or $x(yz)\bar{x}$ (VH); there is no difference between the x and y directions in the Zn_3P_2 unit cell. After careful analysis of the measured spectra, a large number of transitions were found. In the VV case, 33 peaks were observed and 43 peaks for the VH configuration (figures 7 and 8). In the VV configuration the 20 prominent transitions are located in the 26–360

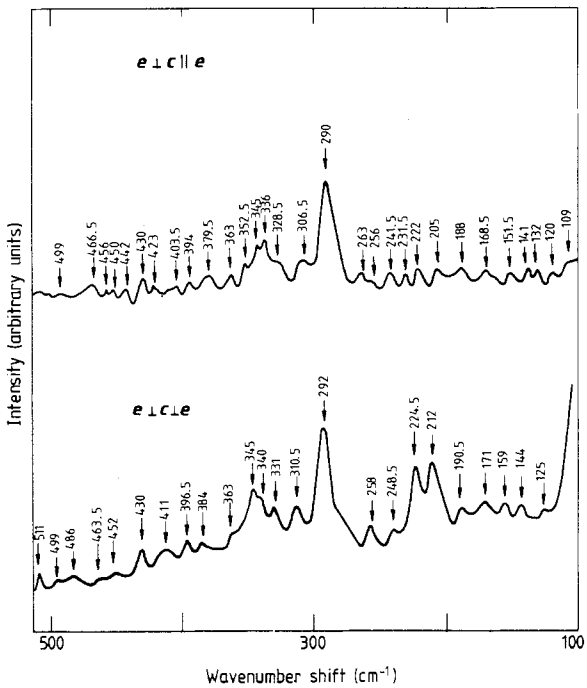

Figure 7. Raman spectra of Zn_3P_2 at room temperature in two configurations: $e \perp c \| e$ (VH), $(y(xz)\bar{y})$, and $e \perp c \perp e$ (VV), $(y(xx)\bar{y})$.

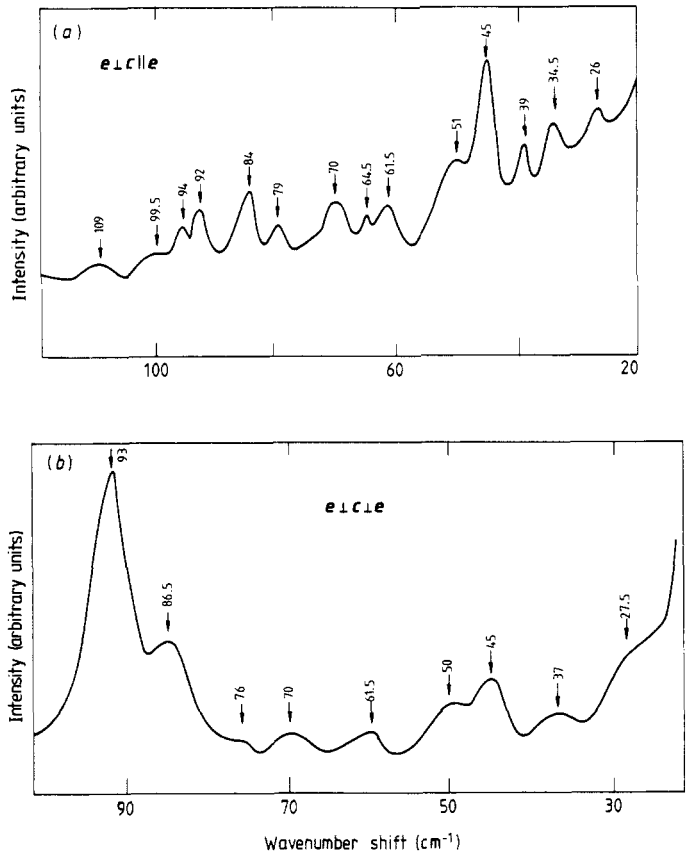

Figure 8. Raman spectra of Zn_3P_2 at room temperature in the low energy range $e \perp c \parallel e$ (VH), $(y(xz)\bar{y}) - a$, and $e \perp c \parallel e$ (VV), $(y(xx)\bar{y}) - b$ configurations, respectively.

cm^{-1} range. Four weaker peaks were also found in this region. In the VH configuration, 28 prominent and five weaker peaks are found in the same region. The wavenumbers of the prominent transitions are collected in table 4.

Finally it should be said that uncertainties in the wavenumber position in the infrared and Raman spectra are $\pm 2\ cm^{-1}$.

5. Discussion

According to the distribution of the Zn_3P_2 modes among the irreducible representations (1, 2), we should expect nine single one-phonon transitions and 15 double-degenerate transitions to be infrared active. From the analysis of reflectivity spectra, we obtain at least 26 one-phonon transitions at room temperature and 32 one-phonon transitions at 10 K (see table 3). On the assumption that, at 295 K, some of the one-phonon transitions are temperature broadened, the total number of 32 observed zone-centred phonons remains in agreement with the total number of permitted phonons. It is necessary to assume that some of the theoretically double-degenerate representations are split.

Raman tensor (4) analysis shows that, in the VV configuration, only nine Γ_1^+ and

Table 5. Infrared overtones at Γ calculated from the data of Table 3 compared with transitions observed in VV Raman scattering (in cm^{-1}).

IR	88	128	141	156	172	206	337	365	492
calculated	114	122	142	157	178	209	338	368	
Raman observed	86.5	125	144	159	171	212	340	363	499

10 Γ_3^+ one-phonon transitions should be visible and, in the VH configuration, 16 Γ_5^+ double-degenerate ones. In the measured VV configuration spectra it is easy to find 20 distinct peaks and to ascribe them to one-phonon branches at Γ. To understand the number of prominent transitions observed in the VH configuration, one has to assume a splitting of the double-degenerate transitions (one-phonon branches at Γ). If we do this, the agreement between theory predictions and experimental results is reasonable. As can be seen in table 4, seven modes are observed in both VV and VH configurations; most of them are located in the low-wavenumber region 26–79 cm^{-1}.

Mutual exclusion rules require, in the case of the crystal with inversion symmetry, that the one-phonon modes observed in infrared and Raman spectra be different. The Zn_3P_2 crystal possesses inversion symmetry and so the same transitions should not be observed. Of the total number of 74 one-phonon transitions in Raman scattering and reflectivity spectra, almost 60 of them are different (compare tables 3 and 4) and thus the rule seems to be well satisfied.

Group theory predicts no overtones of infrared-active phonons at Γ to be allowed in the infrared (see table 1). If only a few coincidences are neglected, this condition is well fulfilled at both 295 and 10 K.

Another theoretical prediction, i.e. that all infrared overtones should be Raman active in the VV configuration, is fulfilled quite reasonably in the measured range (80–500 cm^{-1}). Only a few of the infrared Γ overtones are not consistent with the transitions observed in the Raman spectrum (table 5).

All Raman-active Γ overtones should be Raman active also in the VV configuration, as is indicated in table 1. In the measured spectra we can find most of the expected overtones (table 6); so this condition is quite well fulfilled.

All combinations between infrared-active and Raman allowed transitions at the Γ point should be visible in the infrared (see table 1). As presented in tables 7 and 8, all transitions observed in the two-phonon absorption range may be ascribed to some combinations of the infrared and Raman permitted one-phonon modes.

Table 6. Energies of Raman overtones calculated using table 4 correlated with transitions observed in Raman spectra at the VV configuration (in cm^{-1}).

Calculated	52	69	78	90	102	123	140	158	168		184	218	240	264	282	
	55		74	90	100	123	140			173	186					
Observed	50	70	76	93		125	144	159		171	190	222		258		
Calculated		303		337		376		410		444		463	483			
	288		318		342		381		424		449					516
Observed	292			340	340		384	411			452	463.5	486	511		

Table 7. Energies observed in two-phonon absorption range at 295 K with calculated combinations of the infrared (TO, LO) and Raman (R) zone-centred one-phonons (from tables 3 and 4).

	387		410		425		454		466		480
$LO_1 + R_{35}$	388	$LO_{13} + R_5$	410	$TO_2 + R_{39}$	427	$TO_6 + R_{38}$	455	$TO_6 + R_{36}$	466	$LO_{13} + R_{13}$	480
$LO_{11} + R_7$	388	$TO_2 + R_{37}$	409	$LO_5 + R_{36}$	425	$LO_{13} + R_{11}$	453	$LO_{12} + R_{13}$	465	$TO_{12} + R_{15}$	479
$TO_{12} + R_5$	388	$LO_1 + R_{38}$	409	$TO_{12} + R_{10}$	424.5			$LO_{10} + R_{18}$	466	$TO_{11} + R_{20}$	480.5
	495		530		560		576		588		620
$TO_{13} + R_{16}$	495	$LO_{11} + R_{24}$	532	$TO_{12} + R_{26}$	562	$TO_9 + R_{35}$	577	$TO_9 + R_{37}$	591	$LO_9 + R_{37}$	621
$LO_{10} + R_{21}$	495	$LO_8 + R_{37}$	529	$LO_{12} + R_{24}$	557	$TO_{10} + R_{31}$	575	$LO_{12} + R_{28}$	586.5	$TO_{10} + R_{36}$	621
$LO_8 + R_{33}$	494.5	$LO_{10} + R_{26}$	531.5	$TO_{13} + R_{24}$	563	$TO_{13} + R_{26}$	575.5	$LO_9 + R_{33}$	586.5	$LO_{13} + R_{37}$	618
	646		668		681		690		710		720
$TO_{11} + R_{36}$	646	$LO_{10} + R_{39}$	670	$LO_{11} + R_{39}$	683	$LO_{12} + R_{37}$	690	$LO_{12} + R_{39}$	708	$LO_{13} + R_{39}$	723
$TO_{10} + R_{39}$	648	$TO_{12} + R_{35}$	669	$LO_{12} + R_{36}$	681	$TO_{12} + R_{38}$	690	$LO_{13} + R_{38}$	712		
$TO_{12} + R_{32}$	644.5	$LO_{13} + R_{32}$	666.5	$TO_{13} + R_{35}$	682	$LO_{13} + R_{31}$	691				

Table 8. *Energies observed in two-phonon absorption range at 10 K correlated with calculated combinations of the infrared (TO, LO) at 10 K and Raman (R) at 295 K zone-centred one-phonons (from tables 3 and 4).*

	457		460		468		474		482		499
$LO_5 + R_{39}$	457	$TO_{15} + R_{13}$	460	$TO_{10} + R_{26}$	467.5	$LO_{14} + R_{15}$	474	$LO_8 + R_{33}$	482.5	$TO_8 + R_{34}$	499
$TO_{11} + R_{20}$	456	$TO_8 + R_{31}$	461	$LO_{11} + R_{18}$	469.5	$TO_9 + R_{31}$	474	$TO_{13} + R_{19}$	481	$LO_{10} + R_{26}$	498.5
$TO_{13} + R_{16}$	456.5	$LO_{11} + R_{17}$	461	$LO_{13} + R_{16}$	467	$TO_{10} + R_{27}$	474.5	$LO_{13} + R_{18}$	482	$TO_{14} + R_{19}$	500
$LO_{13} + R_{14}$	457	$LO_{12} + R_{18}$	460.5	$LO_{15} + R_{13}$	468.5	$LO_{13} + R_{17}$	474.5	$TO_{15} + R_{15}$	481	$TO_{15} + R_{18}$	499
	507		523.5		530		561		570		578.5
$TO_{11} + R_{25}$	507	$TO_8 + R_{38}$	522.5	$TO_9 + R_{37}$	529	$TO_{15} + R_{25}$	562	$TO_{13} + R_{29}$	570.5	$LO_{15} + R_{27}$	580
$TO_{12} + R_{23}$	506.5	$LO_8 + R_{38}$	524	$LO_9 + R_{37}$	531	$LO_{15} + R_{24}$	560.5	$TO_{15} + R_{27}$	571.5	$TO_{16} + R_{26}$	578.5
$LO_{15} + R_{18}$	507.5	$LO_{12} + R_{25}$	523.5	$TO_{15} + R_{22}$	530.5	$TO_{16} + R_{23}$	559	$LO_{15} + R_{25}$	570.5		
$LO_{16} + R_{16}$	507	$LO_{14} + R_{22}$	523.5	$LO_{16} + R_{19}$	531.5			$LO_{16} + R_{23}$	568		
	587		595		600		619		626		639
$LO_{13} + R_{30}$	586	$TO_{14} + R_{30}$	594.5	$LO_{11} + R_{31}$	600.5	$LO_{11} + R_{33}$	620	$LO_{10} + R_{38}$	626	$LO_{11} + R_{34}$	638
$TO_{16} + R_{27}$	585.5	$LO_{14} + R_{30}$	596	$TO_{13} + R_{31}$	602.5	$TO_{13} + R_{32}$	619	$LO_{14} + R_{31}$	625	$TO_{14} + R_{32}$	637.5
$LO_{16} + R_{26}$	587.5	$TO_{16} + R_{28}$	595.5	$TO_{15} + R_{29}$	598	$TO_{16} + R_{30}$	617	$LO_{16} + R_{30}$	626	$LO_{14} + R_{32}$	639.5
		$LO_{16} + R_{27}$	594.5			$LO_{16} + R_{29}$	621			$LO_{15} + R_{31}$	638.5
	653		661		679		689		698		705
$LO_{13} + R_{34}$	651.5	$LO_{13} + R_{36}$	659	$TO_{14} + R_{37}$	676.5	$LO_{16} + R_{34}$	671.5	$TO_{16} + R_{37}$	699	$TO_{15} + R_{39}$	703
$LO_{12} + R_{38}$	653.5	$TO_{14} + R_{34}$	660	$LO_{14} + R_{37}$	678	$TO_{16} + R_{36}$	690	$LO_{16} + R_{36}$	699	$TO_{16} + R_{38}$	706
$TO_{15} + R_{33}$	650.5	$LO_{14} + R_{34}$	661.5	$LO_{15} + R_{34}$	677					$LO_{16} + R_{37}$	708
$LO_{16} + R_{31}$	653	$TO_{16} + R_{32}$	660.5								
	715		725								
$TO_{16} + R_{39}$	717	$LO_{16} + R_{39}$	726								
$LO_{16} + R_{38}$	715										

The other transitions observed in Raman spectra in the VV-4 and VH-15 configurations might be explained in terms of one-phonon combinations allowed in the VV or VH configurations. However, one should also take into account transitions at other critical points, predicted by group theory (see table 2).

For energies higher than two-phonon overtones and combinations calculated by using the data from reststrahlen and Raman spectra (tables 3 and 4), one expects three-phonon transitions. In these terms we may explain the spectra presented in figure 6. Three-phonon transition selection rules were not studied in detail. Nevertheless, by means of symmetrised Kronecker cube calculations, we obtain that there are infrared-active three-phonon overtones $[\Gamma_5^-]_{(3)}$ in Γ_5^- and the overtones $[\Gamma_2^-]_{(3)}$ in Γ_2^- polarisations (remember that two-phonon overtones are forbidden in infrared; see table 1). Using this result we can explain most of the transitions in figure 6 (table 9).

Table 9. Three-phonon infrared overtones observed in infrared absorption at 10 K (energy in cm^{-1})

Measured	733		817		861		934		1019		1081	
Calculated from table 3	729	$3TO_{10}$	822	$3LO_{10}$	856	$3TO_{11}$	928.5	$3LO_{11}$	1020	$3TO_{15}$	1089	$3LO_{16}$

There are no theoretical calculations of the phonon spectrum for Zn_3P_2; so we cannot interpret the obtained results in detail yet. By using polarised light in infrared measurements, we shall be able to show which branches belong to LO and TO types and give more information on the Raman-active phonons.

It is also necessary to measure Raman scattering spectra at low temperatures to obtain a much sharper structure than that at room temperature and to discriminate between one-phonon and multi-phonon transitions. It is very important to understand the physical reason for the splitting of doubly degenerate modes at the Γ point. A cause of this might be connected with the displacements of the atomic positions in the ideal anti-fluoride cell. The other explanation might be based on the fact that in the Zn_3P_2 unit cell the same atoms are located in a few different crystallographic positions. This may cause some perturbation in the lattice dynamics.

There are only a few data on lattice vibrations in other $A_3^{II}B_2^{V}$ compounds, i.e. Cd_3P_2, Cd_3As_2 and Zn_3As_2. For Cd_3P_2 (a compound isostructural with Zn_3P_2), reflectivity spectra were presented only within the 150–450 cm^{-1} range at several temperatures by Gelten and Van Es (1984). Comparing our reflectivity plots for Zn_3P_2 with those of Cd_3P_2, we find the same number of reflectivity peaks in both spectra. This is expected owing to the same symmetry of both crystals.

More data are available for Cd_3As_2 crystals of C_{4v}^{12} symmetry. The infrared reflectivity of Cd_3As_2 was measured by Gelten and Van Es (1981), Thielmann *et al* (1981) and Houde *et al* (1986). These papers present reflectivity spectra in the 120–400 cm^{-1} range. The most interesting spectrum consisting of at least 11 features was presented by Houde *et al* (1986). In the other two papers, only a few (three and five, respectively) modes were observed.

Raman scattering was measured for Cd_3As_2 by Jandl *et al* (1984). In this study, nine features were observed in the spectrum. The very small numbers of modes observed are in sharp contrast with the number of infrared-active modes expected for this compound. This discrepancy is explained by weak dipolar moments and polarisability tensors in the Cd_3As_2 structure (Jandl *et al* 1984, Houde *et al* 1986).

For the Zn_3As_2 layers grown by MBE, Raman scattering spectra were measured in the 20–260 cm^{-1} range by Pangilinan *et al* (1989). More than 30 modes were observed in these spectra for different light polarisations. The higher quality of the Zn_3As_2 layers may give better resolution of the Raman spectra for Zn_3As_2 in comparison with Cd_3As_2 (Jandl *et al* 1984). There is also a distinct difference between the carrier concentrations in the semiconductors discussed above; from 10^{18} cm^{-3} for Cd_3As_2, through 10^{17}–10^{18} cm^{-3} for Cd_3P_2 and Zn_3As_2 to about 10^{13} cm^{-1} for the Zn_3P_2 crystals used in the present paper (all data are at room temperature). This small free-carrier concentration value may correlate with the high resolution of the Zn_3P_2 lattice mode spectra.

6. Summary

The symmetry of the infrared- and Raman-active one-phonon branches for Zn_3P_2 was determined on the basis of group theory. Critical point analysis and compatibility relations allowed us to find the symmetry of phonon branches through the symmetry lines and points in the Brillouin zones. Selection rules of the overtones and combinations for all high-symmetry points were derived. The theoretical results were applied to interpret the experimental results.

The experimental part of this paper presents, for the first time, Raman scattering spectra of Zn_3P_2 and reflectivity and absorption spectra in the whole fundamental vibration range (40–1200 cm^{-1}). From the reflectivity results the set of infrared-active one-phonon modes was determined. The main transitions in Raman spectra were also ascribed to one-phonon branches at the Γ point. The other Raman transitions and singularities in the absorption spectra were interpreted in terms of overtones and two-phonon combination bands. Most of the theoretical predictions match the experimental results well, which leads us to the conclusion that the Zn_3P_2 crystal symmetry cannot be simplified to any cubic structure.

Acknowledgments

The author is deeply indebted to Dr D Heiman from the Francis Bitter National Magnet Laboratory, MIT, Cambridge, MA, USA, who made it possible for him to perform Raman scattering experiments as well as to Dr J M Wrobel and B P Clayman from Simon Fraser University, Burnaby, Canada, for help with the far-infrared measurements. A critical reading of the manuscript by Professor J M Pawlikowski from the Technical University of Wrocław is also acknowledged. This work was supported by the Polish Academy of Sciences under Contract CPBP 01.04.I. 2.7.

References

Barker A S 1970 *Far Infrared Properties of Solids* ed. S S Mitra and S Nudelman (New York: Plenum) p 247

Bendett M P and Hungspreger R G 1981 *J. Electron. Mater.* **10** 559–64

Birman J L 1984 *Theory of Crystal Space Groups and Lattice Dynamic* ed. L Genzel (Berlin: Springer) pp 220–31

Bouckaert L P, Smoluchowski R and Wigner E 1936 *Phys. Rev.* **50** 58–66

Fagen E A 1979 *J. Appl. Phys.* **50** 6505–15

Fateley W G, McDevitt N T and Bentley F F 1971 *Appl. Spectrosc.* **25** 155–73

Gelten M J and Van Es C M 1981 *Proc. 4th Int. Conf. Physics of Narrow Gap Semiconductors (Linz)* ed. E Gornik, H Heinrich and L Palmetshofer (Berlin: Springer) pp 167–71
—— 1984 *J. Phys. C: Solid State Phys.* **17** 3721–8
Houde D, Jandl S, Banville M and Aubin M J 1986 *Solid State Commun.* **57** 247–8
Jandl S, Desgreniers S, Carlone C and Aubin M H 1984 *J. Raman Spectrosc.* **15** 137–8
Kovalev O V 1965 *Irreducible Representations of Space Groups* (New York: Gordon and Breach) pp 46–84
Loferski J J 1956 *J. Appl. Phys.* **27** 777–87
Loudon R 1964 *Adv. Phys.* **13** 423–82
Misiewicz J and Gaj J 1981 *Phys. Status Solidi* b **105** K23–5
Misiewicz J and Królicki F 1985 *Mater. Sci.* **11** 39–55
Misiewicz J, Królicki F, Lewicki M and Kasprzak J F 1986b *Acta Phys. Polon.* A **69** 1127–30
Misiewicz J, Mirowska N and Gumienny Z 1984 *Phys. Status Solidi* a **83** K51–6
Misiewicz J, Sujak-Cyrul B and Bartczak A 1986a *Solid State Commun.* **58** 677–9
Misiewicz J, Wrobel J M and Clayman B P 1988 *Solid State Commun.* **66** 747–50
Mooser E and Pearson W B 1961 *Prog. Semicond.* **5** 103–40
Mulliken R S 1933 *Phys. Rev.* **43** 278
Nauka K and Misiewicz J 1981 *Phys. Status Solidi* a **65** K95–7
Pangilinan G, Sooryakumar R, Chelluri B and Chang T Y 1989 **62** 551–5
Pawlikowski J M 1982 *Phys. Rev.* B **26** 4711–3
—— 1988a *Infrared Phys.* **28** 177–82
—— 1988b *Rev. Solid State Sci.* **2** 581–602
Pawlikowski J M, Misiewicz J and Mirowska N 1979 *J. Phys. Chem. Solids* **40** 1027–33
Pistorius C W F T, Clark J B, Coetzner J, Kruger G J and Kunze O A 1977 *High Temp.–High Pressures* **9** 471–82
Radautsan R S, Syrbu N N, Nebola J J and Volodina V J 1988 *Sov. Phys.–Solid State* **19** 1290
Stackelberg M and Paulus R 1935 *Z. Phys. Chem.* B **24** 427–60
Streitwolf H W 1967 *Gruppentheorie in der Festkörperphysik* (Leipzig: Akademishe Verlagsgesellschaft Geest und Portig K-G) 143–6
Thielmann J, Ortenberg M V, Blom F A P and Strobel K 1982 *Proc. 4th Int. Conf. Physics of Narrow Gap Semiconductors (Linz) 1981, Lecture Notes in Physics* vol 152, ed. E Gornik, H Heinrich and L Palmetshofer (Berlin: Springer) pp 207–11
Wrobel J M and Misiewicz J 1989 to be published
Żdanowicz W and Żdanowicz L 1975 *Ann. Rev. Mater. Sci.* **5** 301–27